Journal of Applied Physics

RESEARCH ARTICLE | OCTOBER 06 2022

Enhancement of the anomalous Nernst effect in epitaxial Fe_4N films grown on $SrTiO_3$(001) substrates with oxygen deficient layers

Keita Ito; Jian Wang; Yusuke Shimada; ... et. al

Journal of Applied Physics 132, 133904 (2022)
https://doi.org/10.1063/5.0102928
CHORUS

Journal of Applied Physics | ARTICLE | scitation.org/journal/jap

Enhancement of the anomalous Nernst effect in epitaxial Fe_4N films grown on $SrTiO_3$(001) substrates with oxygen deficient layers

Cite as: J. Appl. Phys. **132**, 133904 (2022); doi: 10.1063/5.0102928
Submitted: 26 June 2022 · Accepted: 7 September 2022 ·
Published Online: 6 October 2022

Keita Ito,[1,2,a)] Jian Wang,[1,2,b)] Yusuke Shimada,[1] Himanshu Sharma,[1,3,c)] Masaki Mizuguchi,[1,2,3,d)] and Koki Takanashi[1,2,4,e)]

AFFILIATIONS

[1]Institute for Materials Research, Tohoku University, Sendai 980-8577, Japan
[2]Center for Spintronics Research Network, Tohoku University, Sendai 980-8577, Japan
[3]CREST, Japan Science and Technology Agency, Kawaguchi 332-0012, Japan
[4]Center for Science and Innovation in Spintronics, Core Research Cluster, Tohoku University, Sendai 980-8577, Japan

[a)]**Author to whom correspondence should be addressed:** keita.ito.e3@tohoku.ac.jp
[b)]**Present address:** Magnetic Powder Metallurgy Research Center, National Institute of Advanced Industrial Science and Technology, Nagoya 463-8560, Japan
[c)]**Present address:** Imec, Kapeldreef 75, B-3001 Leuven, Belgium, and Department of Chemistry, KU Leuven, Celestijnenlaan 200f, 2404, 3001 Leuven, Belgium
[d)]**Present address:** Institute of Materials and Systems for Sustainability/Department of Materials Process Engineering, Graduate School of Engineering, Nagoya University, Nagoya 464-8603, Japan, and Center for Spintronics Research Network, Osaka University, Toyonaka 560-8531, Japan
[e)]**Present address:** Advanced Science Research Center, Japan Atomic Energy Agency, Tokai 319-1195, Japan

ABSTRACT

Anomalous Nernst effect of epitaxial Fe_4N films on MgO(001), $MgAl_2O_4$(MAO)(001), and $SrTiO_3$(STO)(001) substrates grown by molecular beam epitaxy was investigated. Moderately large anomalous Nernst coefficients (S_{ANE}) of 1.4 and 1.7 μV/K were obtained in the Fe_4N films on the MgO(001) and MAO(001) substrates, respectively, and large anomalous Hall angles (~0.06) and transverse thermoelectric conductivities [~1.3 A/(m K)] were derived from the experimental results. On the other hand, a large effective S_{ANE} of 2.8 μV/K was obtained in the Fe_4N film on the STO(001) substrate. The origin of the enhanced effective S_{ANE} is the negatively large Seebeck coefficient (S_{SE}) in an oxygen deficient STO layer near the surface of the STO substrate. This indicates that it is possible to enhance the effective S_{ANE} of ferromagnetic materials by utilizing adjacent materials with large $|S_{SE}|$ such as the oxygen deficient STO layer.

I. INTRODUCTION

Green energy harvesting technologies, which convert micro energy from waste heat, solar light, and environmental sound into electric power, play an important role in a global sustainable energy solution. Recently, the development of thermoelectric power generation (TEG) devices utilizing the anomalous Nernst effect (ANE) is attracting increasing interest with its unique merits compared with the conventional Seebeck effect (SE)-based TEG.[1–5] ANE is a thermoelectric phenomenon, where an electromotive force is generated in the direction orthogonal to both a temperature gradient (∇T) applied to a ferromagnetic material and its magnetization.[1] Semiconductor thermoelectric conversion devices that utilize the SE require *p-n* junction arrays with a complicated structure.[5] On the other hand, thermoelectric conversion devices using

ANE can be realized with a simple single-layer ferromagnetic film and have advantages such as a large area coverage, low cost, and voltage output in the direction orthogonal to ∇T.[2–5] Thereby, it is an energy harvesting technology that has a high degree of freedom in non-flat heat source surface and installation locations and has a very high affinity with independent power sources for light, temperature, humidity, current, magnetic field (H), and pressure sensors. However, a current critical technical issue for practical applications of ANE-based TEG is the much small value of the thermoelectric power of ANE compared with that of the conventional SE-based TEG.[5]

Generally, the dimensionless figure of merit (ZT) is used as a parameter indicating the performance of the thermoelectric devices, and it is expressed as $ZT = \sigma S_{\mathrm{ANE}}^2/\kappa$ in the ANE-based TEG devices.[4] Here, σ, S_{ANE}, and κ are the electrical conductivity, the anomalous Nernst coefficient, and the thermal conductivity of a ferromagnetic material, respectively. According to the Wiedemann–Franz law,[6] since σ/κ is constant in an isotropic substance, it is generally difficult to achieve both a large σ and a small κ in metals to achieve a high ZT. Therefore, to realize high-performance ANE-based TEG devices, exploring a material with a large S_{ANE} is essential. S_{ANE} is represented by $S_{\mathrm{ANE}} = \rho_{xx}\alpha_{xy} + \rho_{xy}\alpha_{xx}$, where ρ_{xx}, ρ_{xy}, α_{xx}, and α_{xy} are the longitudinal resistivity, the transverse resistivity, the longitudinal thermoelectric conductivity, and the transverse thermoelectric conductivity, respectively.[7,8] From the definitions of the anomalous Hall angle, $\tan\theta_{\mathrm{AHE}} = \rho_{yx}/\rho_{xx}$ $(= -\rho_{xy}/\rho_{xx})$, and the Seebeck coefficient, $S_{\mathrm{SE}} = \rho_{xx}\alpha_{xx}$, we obtain the following equation:[7]

$$S_{\mathrm{ANE}} = S_{\mathrm{I}} + S_{\mathrm{II}} = \rho_{xx}\alpha_{xy} - S_{\mathrm{SE}}\tan\theta_{\mathrm{AHE}}. \tag{1}$$

Therefore, to realize a large S_{ANE} value, $\rho_{xx}\alpha_{xy}$ $(= S_{\mathrm{I}})$ and $-S_{\mathrm{SE}}\tan\theta_{\mathrm{AHE}}$ $(= S_{\mathrm{II}})$ with the same sign and large absolute values is required. Here, S_{I} is the term indicating the intrinsic ANE generated by converting ∇T into a transverse electrical field by α_{xy}, and S_{II} is the term due to the transverse carrier flow generated by the combination of SE and the anomalous Hall effect (AHE) in a sample.[5]

Sakai *et al.*[9] predicted the α_{xy} values of more than 250 types of Fe-based binary ferromagnetic materials, which are abundant in resources and highly practical, by a high-throughput calculation method based on the first-principles calculations. Among them, there are five promising materials with large α_{xy} which are Fe_3Pt [6.2 A/(m K)], Fe_3Ga [3.0 A/(m K)], Fe_3Al [2.7 A/(m K)], Fe_3Si [2.5 A/(m K)], and Fe_4N [2.4 A/(m K)]. In Ref. 9, S_{ANE}, S_{SE}, and $\tan\theta_{\mathrm{AHE}}$ were measured by experiments on bulk and film samples of Fe_3Ga and Fe_3Al, and α_{xy} was obtained from Eq. (1). However, for other promising materials, i.e., Fe_3Pt, Fe_3Si, and Fe_4N, α_{xy} has not been evaluated experimentally, and only S_{ANE} of Fe_4N films was reported.[4,10] Isogami *et al.*[10] grew epitaxial Fe_4N films on MgO(001) substrates by a sputtering method and performed ANE measurements. A relatively large S_{ANE} of 2.2 μV/K was demonstrated when H was applied in the direction perpendicular to the film surface and ∇T was applied to the in-plane Fe_4N[110] direction.

In this study, large effective S_{ANE} of 2.8 μV/K has been achieved in epitaxially grown Fe_4N films on $SrTiO_3$(STO)(001) substrates, which have a conductive oxygen deficient layer with a negatively large S_{SE} value[11] near its surface. This suggests that the effective S_{ANE} of ferromagnets can be enhanced by stacking with a material showing a large $|S_{\mathrm{SE}}|$, as can be explained with Eq. (1). In this paper, S_{ANE} modulated by adjacent materials with large $|S_{\mathrm{SE}}|$ is referred to as "effective S_{ANE}." On the other hand, since it was difficult to evaluate the amount of shunt current to the oxygen deficient layer, thus it was further difficult to accurately evaluate ρ_{xx}, ρ_{xy}, and α_{xy} of these samples using Eq. (1). Therefore, epitaxial Fe_4N films were also prepared on insulating MgO(001) and $MgAl_2O_4$(MAO) (001) substrates, with which α_{xy} of Fe_4N were evaluated.

II. EXPERIMENTAL METHOD

The Fe_4N films were grown on MgO(001) (sample A), MAO (001) (sample B), and STO(001) (samples C–E) substrates by the plasma-assisted molecular beam epitaxy (MBE) technique. The substrates, the thicknesses, and the growth temperatures of the Fe_4N films are summarized in Table I. Fe and N were simultaneously supplied by an electron beam gun and radio-frequency plasma gun, respectively.[12,13] Subsequently, a 2-nm-thick Al capping layer was formed on the Fe_4N layers in a sputtering chamber connected to the MBE chamber. The Al layer was oxidized by natural oxidation after air exposure. The crystallographic structures of the samples were confirmed by x-ray diffraction (XRD) measurements using a Cu-Kα radiation source (SmartLab: Rigaku Corp.) and cross-sectional high-angle annular dark-field scanning transmission electron microscope (HAADF-STEM) observation (JEM-ARM200F: JEOL Ltd.), and the film thicknesses were confirmed by the x-ray reflectivity method. After the XRD measurements, the samples were microfabricated into a Hall bar shape using photolithography and ion milling for the measurement of ANE, SE, and AHE. A schematic illustration of the measurement setup is shown in Fig. 1, which is the same as reported in Refs. 14 and 15. The distance between the Seebeck voltage (V_{SE}) electrodes was 5.0 mm and that between the Nernst voltage (V_{ANE}) electrodes was 2.2 mm. Next, on-chip thermometers[14–17] were fabricated by ion beam sputtering and a lift-off technique. The structure of the on-chip thermometers was a meandering shape Cr(10 nm)/Pt(150 nm) wire with the width of 20 μm. Finally, electrode pads of Cr(10 nm)/Au(200 nm) were formed by ion beam sputtering and the lift-off technique. The prepared samples were pasted by thermal grease on Cu blocks of a homemade holder, and thermoelectric measurements were performed using the external control option of a physical property measurement system (PPMS: Quantum Design Inc.) while ∇T was applied along to the longitudinal direction of the Hall bar (in-plane Fe_4N[110] direction) with a heater bonded to the Cu block. The ambient temperature was about 310 K and the temperature difference (ΔT) was varied by

TABLE I. The substrates, the thicknesses, and the growth temperatures of the Fe_4N films in the samples A–E.

	Substrate	Thickness (nm)	Growth temperature (°C)
Sample A	MgO(001)	27	450
Sample B	MAO(001)	27	450
Sample C	STO(001)	27	450
Sample D	STO(001)	27	400
Sample E	STO(001)	17	450

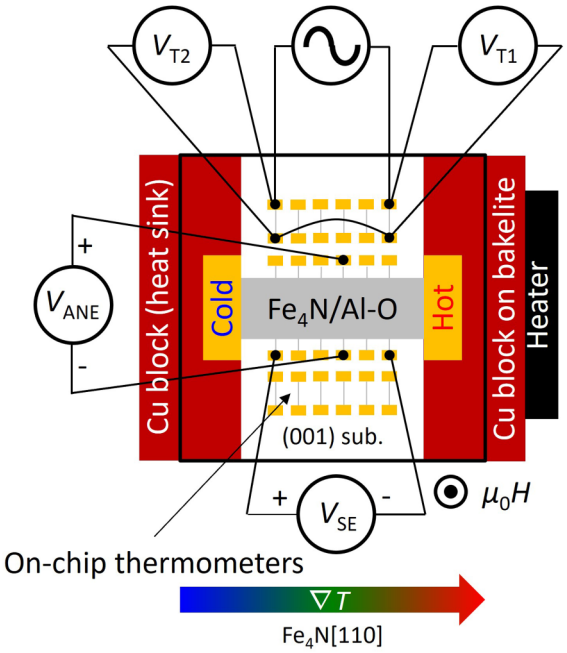

FIG. 1. A schematic illustration of the sample setup for the thermoelectric measurements in this study.

tuning the heater voltages. An external H ($\mu_0 H = -3 \sim +3$ T) was applied with the direction perpendicular to the film surface, and V_{SE} and V_{ANE} were measured using nanovoltmeters (Keithley Nanovoltmeter Model 2182A: Keithley Instruments Inc.). ΔT was estimated by simultaneously measuring the voltage of the on-chip thermometers on the heater side (V_{T1}) and the heat sink side (V_{T2}) by the four-probe method with two lock-in amplifiers (LI5650: NF Corp.) during the thermoelectric measurements. For the calibration of ΔT, the temperature dependence of the electrical resistance (R) for each on-chip thermometers both on hot and cold sides were measured in the range of 300–360 K using PPMS, separately from the thermoelectric measurement. In the R–T curves of the on-chip thermometers, good linearities were confirmed and their slopes were used for real-time calculation of ΔT. The AHE of the samples were measured by PPMS applying external H ($\mu_0 H = -3 \sim +3$ T) in the direction perpendicular to the films at 310 K.

III. RESULTS AND DISCUSSIONS

A. Structural characterizations of the Fe_4N films

Figures 2(a)–2(c) present the out-of-plane and in-plane XRD patterns of the samples A–C, respectively. In the in-plane XRD measurements, the direction of the scattering vector was along [100] of the substrates. The diffractions of Fe_4N 001 and 002 were obtained in the out-of-plane XRD patterns (red lines), and the peaks of Fe_4N 100 and 200 were observed in the in-plane XRD patterns (blue lines) in Figs. 2(a)–2(c), which indicated that the Fe_4N films were epitaxially grown on MgO(001), MAO(001), and STO(001)

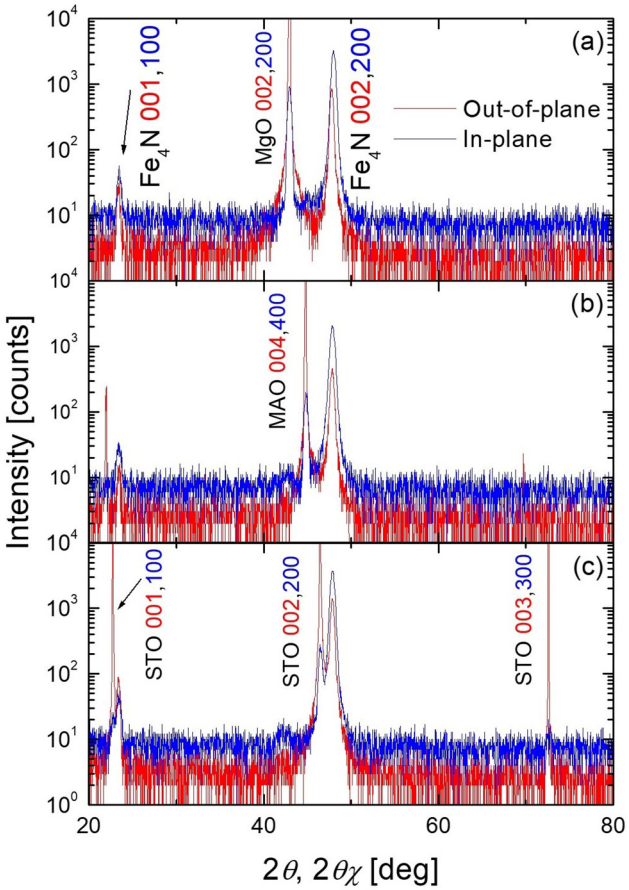

FIG. 2. The out-of-plane (red lines) and the in-plane (blue lines) XRD patterns of the samples (a) A, (b) B, and (c) C.

with a cube-on-cube epitaxial relationship (Fe_4N(001)[100]// sub.(001)[100]). The in-plane and out-of-plane lattice constants (a and c) of the Fe_4N layers were near the bulk value. The lattice mismatches of MgO(001)/Fe_4N, MAO(001)/Fe_4N, and STO(001)/ Fe_4N are −9.9, −6.0, and −2.8%, respectively.[13] However, there was almost no lattice distortion in the samples A–C, and similar results were obtained for the samples D and E.

Figures 3(a)–3(c) indicate the cross-sectional HAADF-STEM images of the samples A–C viewed along the [100] zone axis of the substrates. High-resolution lattice images of the Fe_4N layers with good epitaxial interface were observed for all the samples. Figures 3(d)–3(f) are the fast Fourier transform (FFT) images, which corresponding to the electron diffraction patterns of the Fe_4N layers and the substrates. From these FFT images, the cube-on-cube epitaxial relationship of Fe_4N(001)[100]//sub.(001) [100] was also confirmed. Figures 3(g)–3(i) show the inverse FFT images of Figs. 3(d)–3(f), respectively. The yellow markers in the inverse FFT images indicate the misfit dislocations, which is directly above the substrates, so that lattice relaxation occurs at

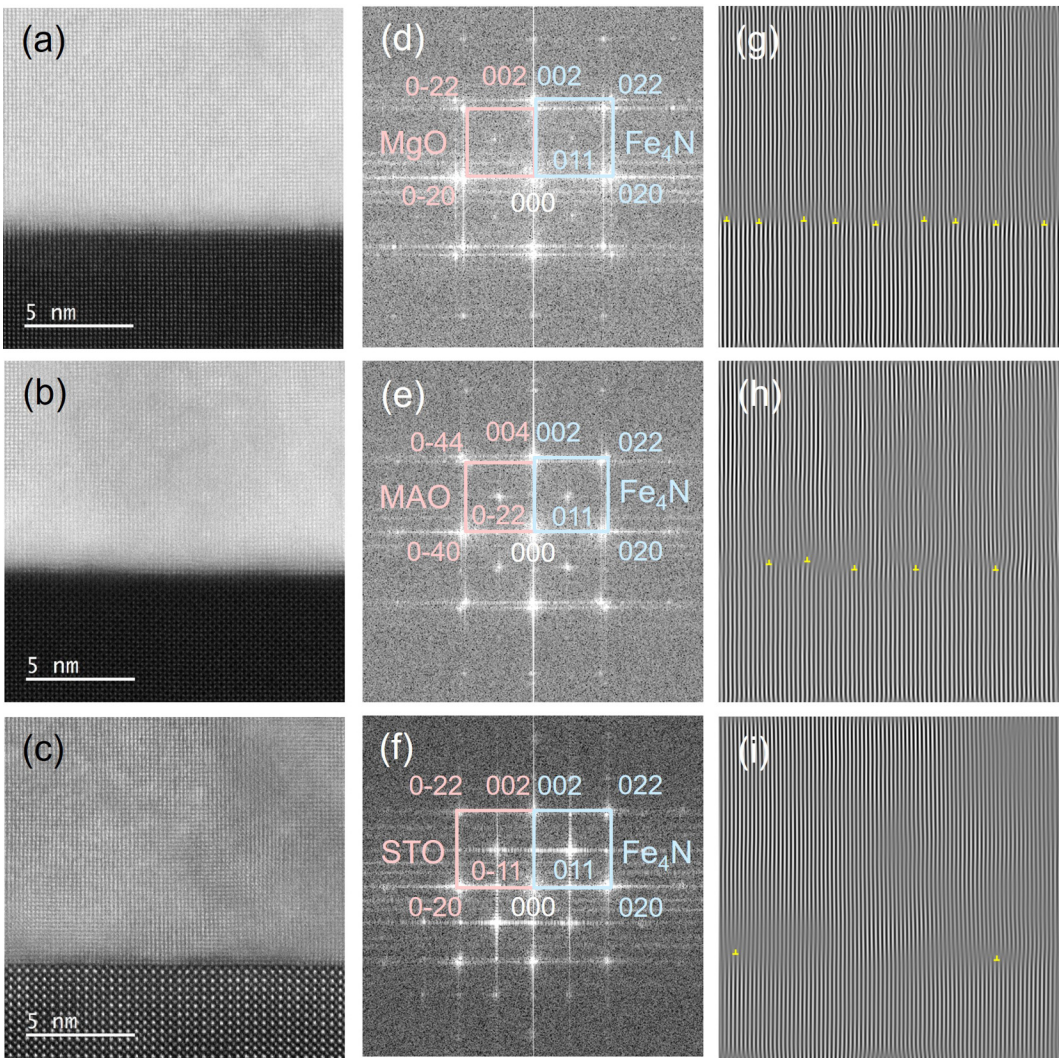

FIG. 3. The cross-sectional HAADF-STEM images of the samples (a) A, (b) B, and (c) C viewed along the [100] zone axis of the substrates. (d)–(f) are the FFT images, and (g)–(i) are the inverse FFT images of (d)–(f), respectively. The yellow markers indicate the positions of misfit dislocations.

the interface with Fe_4N for all the samples. Therefore, the degree of lattice distortion is negligibly small, and it is consistent with the result of $c/a = 1$ obtained from the XRD measurements. The density of the misfit dislocations decreased with the lattice mismatch between Fe_4N and the substrate.

B. Anomalous Hall effect in the Fe_4N films

The ρ_{xx} values of the samples A–E were 102, 115, 82, 96, and 93 $\mu\Omega$ cm, respectively. The ρ_{xx} values of the samples on STO (samples C–E) were smaller than those of the samples on MgO and MAO (samples A and B). Here, it is suggested that the surface of the STO is conductive, and the current is shunting to the STO substrate. It has long been known that the STO becomes conductive and exhibits a negatively large S_{SE} value when oxygen vacancies are introduced.[11] Oxygen deficiencies might be introduced during the film growth process of the Fe_4N layers at 400 and/or 450 °C. Therefore, the obtained ρ_{xx} and ρ_{yx} values of the samples C–E are underestimated and inaccurate. Since the thickness and electron concentration of the oxygen deficient STO layer cannot be estimated, it is extremely difficult to evaluate the accurate ρ_{xx} and ρ_{yx} of the Fe_4N layer by estimating the specific resistance of the oxygen deficient STO layer. One might concern that this current shunting also affects the evaluations of S_{SE} and S_{ANE} values of the samples C–E. However, it was difficult to estimate the shunting effect in thermoelectric measurements. Therefore, the Fe_4N and the oxygen deficient STO layers were regarded as one material when the S_{SE} and S_{ANE} values of the samples C–E

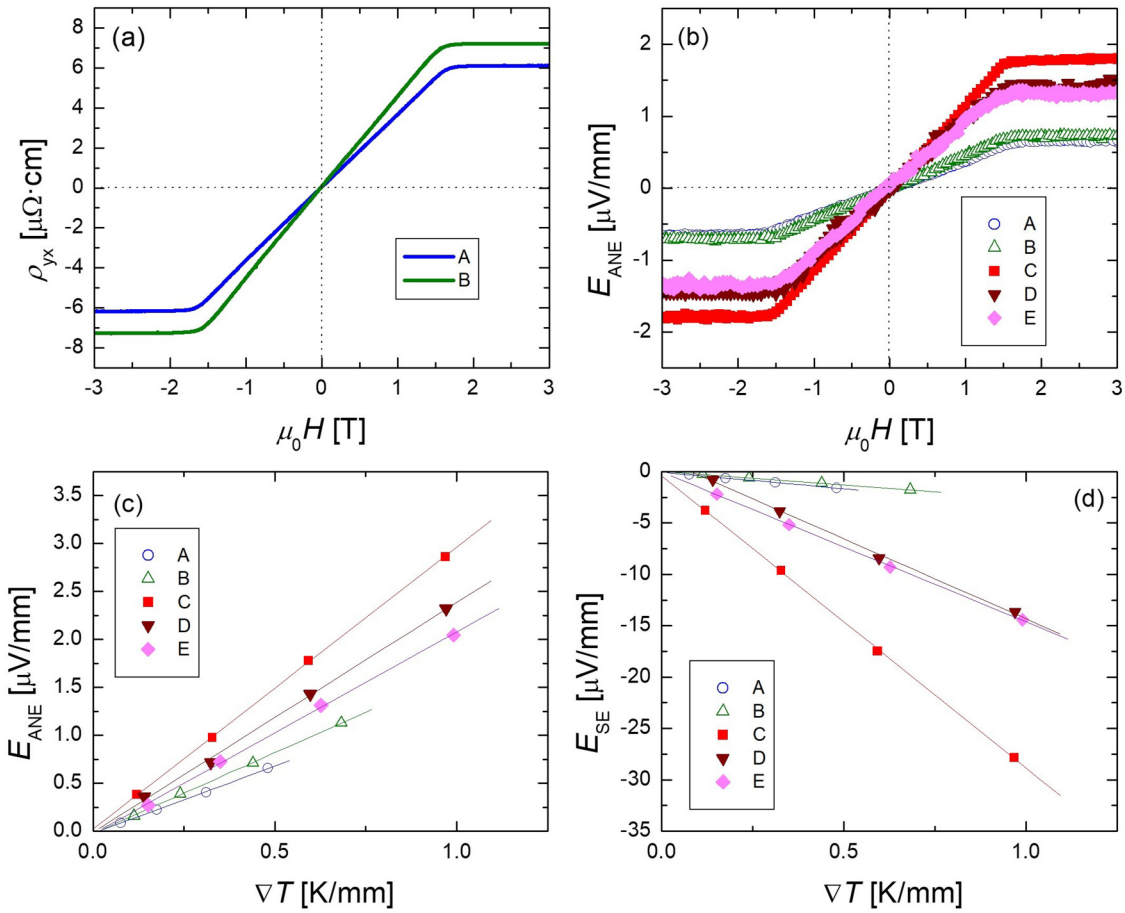

FIG. 4. (a) The external H dependences of ρ_{yx} for the samples A and B in the AHE measurements. (b) The external H dependences of E_{ANE} of the samples A–E at $\nabla T \sim 0.5$ K/mm. (c) ∇T vs E_{ANE} and (d) ∇T vs E_{SE} plots of the samples A–E. The solid lines are results of linear fits.

were evaluated (described later). According to the comparison among the samples C–E, the decrease of ρ_{xx} is the largest in the sample C, which has a relatively higher film growth temperature and a longer growth duration time (large thickness). It means that the magnitude of the shunt current increases with the growth temperature and duration time. It was reported that oxygen vacancies in STO substrates were formed during the film growth process on them,[18] and it is reasonable that the amount of oxygen deficiency in the STO substrate changes depending on the growth conditions of the Fe_4N layers. The oxygen deficiency in the STO substrate was also suggested by the results of thermoelectric measurements described later.

Figure 4(a) shows the external H dependence of $\rho_{yx}(=-\rho_{xy})$ for the samples A and B. The ρ_{yx} values of the samples A and B are 6.1 and 7.2 $\mu\Omega$ cm, respectively, and the $\tan\theta_{AHE}$ values of the samples A and B were calculated to be 0.060 and 0.063, respectively. The materials showing large AHE are useful for applications in spintronics devices. It should be noted that these $\tan\theta_{AHE}$ values are in good agreement with the reported values[19,20] and several times larger than those of conventional ferromagnetic materials such as Fe (0.009) and Co (0.005).[21]

C. Anomalous Nernst effect in the Fe_4N films

Figure 4(b) displays the external H dependences of the electric field due to ANE ($E_{ANE} = V_{ANE}$/Hall bar width) of the samples A–E when ∇T is around 0.5 K/mm. The curve shape corresponding to Fig. 4(a) was observed for all the samples. Figures 4(c) and 4(d) indicate the plots of ∇T vs E_{ANE} and ∇T vs E_{SE} ($E_{SE} = V_{SE}$/Hall bar length), respectively, for the samples A–E. S_{ANE} and S_{SE} of the samples A–E were obtained from the slopes of the linear fitting curves and summarized in Table II. The S_{ANE} values of the Fe_4N films grown on STO(001) (samples C–E) were larger than those of the Fe_4N films on MgO(001) and MAO(001) (samples A and B). The S_{ANE} value of 2.8 μV/K was obtained in the sample C, which was almost twice of the S_{ANE} values in the samples A and B fabricated under the same growth conditions. The S_{SE} value of sample C was −27.3 μV/K, which was about 10 times larger in magnitude

TABLE II. The experimentally obtained S_{ANE}, S_{SE}, S_I ($=\rho_{xx}\alpha_{xy}$), S_{II} ($=-S_{SE}\tan\theta_{AHE}$), α_{xy} values of the samples. × means values which cannot be evaluated due to inaccuracy of ρ_{xx} and ρ_{xy} values of the Fe_4N layers on the oxygen deficient STO layers.

	S_{ANE} (μV/K)	S_{SE} (μV/K)	S_I (μV/K)	S_{II} (μV/K)	α_{xy} [A/(m K)]
Sample A	1.4 ± 0.1	−2.9 ± 0.2	1.2	0.2	1.2
Sample B	1.7 ± 0.1	−2.6 ± 0.1	1.5	0.2	1.3
Sample C	2.8 ± 0.1	−27.3 ± 0.2	×	×	×
Sample D	2.3 ± 0.1	−15.4 ± 0.5	×	×	×
Sample E	2.2 ± 0.1	−15.2 ± 0.4	×	×	×

than those of the samples A and B. This is because the negatively large S_{SE} in the oxygen deficient STO layer enhances S_{SE} of the whole sample. In the samples D (the low growth temperature sample) and E (the short growth duration time sample), the $|S_{SE}|$ values were smaller than that of the sample C. These results also imply that the negatively large S_{SE} is caused by the formation of the oxygen deficient layer of the STO substrate, depending on the growth conditions of the Fe_4N layers. The formation of oxygen vacancies in STO substrates was reported in different previous papers.[11,18,22–25] One of the papers reported[25] that oxygen vacancies were formed even at the temperature of 350 °C by ultraviolet irradiation. When the Fe_4N layers were grown, N plasma was supplied by a radio-frequency plasma gun. Meanwhile, STO was irradiated by ultraviolet rays. Therefore, it is possible that this ultraviolet irradiation introduces oxygen vacancies on the surface of the STO substrate. The observation of concentration distribution for oxygen atoms near the STO surface was attempted by energy dispersive x-ray spectroscopy with the STEM measurement (STEM-EDS). However, no change of the oxygen concentration was detected within the present limited sensitivity of STEM-EDS. As another mechanism for increasing S_{SE}, the effect of lattice strain was also reported.[14,26] However, no effect of the lattice strain is detected from the results of the XRD and HAADF-STEM measurements. Considering Eq. (1), we may conclude that this enhancement of the negative S_{SE} is a dominant reason why the larger S_{ANE} was obtained in the STO(001)/Fe_4N samples. In other words, the scenario is that the longitudinal current generated by large SE in the oxygen deficient STO layers flows into the Fe_4N layer and is converted into a lateral current by the AHE in the Fe_4N layer. Here, S_{ANE} modulated by adjacent materials with large $|S_{SE}|$ is referred to as "effective S_{ANE}." Uchida *et al.*[5] summarize S_{ANE} values of various materials, and the value of 2.8 μV/K of the sample C exceeds the S_{ANE} value of FePt (2.4 μV/K)[27] and comparable with that of $Fe_{81}Al_{19}$ (3.4 μV/K).[28] This result suggests that STO(001)/Fe_4N is promising as a film material showing a large ANE. Utilizing the oxygen deficient STO layer showing a negatively large S_{SE} is an effective method to enhance the effective S_{ANE} of ferromagnetic films. However, it should be noted that effective S_{ANE} might be compensated depending on the combination of the signs of S_I and S_{II} in ferromagnetic materials.

Finally, using the experimental results of the samples A and B, where the accurate ρ_{xx} and ρ_{xy} values were evaluated, α_{xy} of Fe_4N was derived. In Table II, S_I, S_{II}, and α_{xy} values of the samples A and B are summarized. By substituting S_{ANE}, S_{SE}, ρ_{xx}, and $\tan\theta_{AHE}$ obtained in the measurements into Eq. (1), α_{xy} of the samples A and B were estimated to be 1.2 and 1.3 A/(m K), respectively. These values are of the same order as the theoretically predicted 2.4 A/(m K).[9] The experimentally obtained α_{xy} values here are as large as those of promising materials showing large ANE such as $Fe_{1-x}Ga_x$ and $Co_2MnAl_{1-x}Si_x$.[29,30] S_I is larger than S_{II}, and it is considered that large α_{xy} contributes to large S_{ANE} in Fe_4N. Further enhancement of α_{xy} and S_{ANE} is a future problem and might be realized by fabrication of multilayer nanostructures with non-magnetic materials.[14,31–34] In addition, a large α_{xy} is also expected in Mn_4N,[35] suggesting that the magnetic nitrides are promising candidates as large ANE materials.

IV. SUMMARY

In summary, epitaxial Fe_4N films were prepared on MgO (001), MAO(001), and STO(001) substrates by MBE, and the corresponding ANE, SE, and AHE were studied. The results reveal that Fe_4N is a promising material showing a large AHE and ANE and its effective S_{ANE} can be enhanced using the oxygen deficient STO layer showing a negatively large S_{SE}. This is a convenient way to enhance the effective S_{ANE} of ferromagnetic films.

ACKNOWLEDGMENTS

We thank T. Seki, W. Zhou, and Y. Sakuraba for technical support to measure ANE, and T. Sasaki for her help doing the film deposition by ion beam sputtering. This work was supported by the Grants-in-Aid for Scientific Research (C) (Grant No. JP21K04859) and (S) (Grant Nos. JP18H05246 and JP21H05016) from JSPS KAKENHI, JST-CREST (Grant No. JPMJCR1524), the Murata Science Foundation, CASIO Science Promotion Foundation (37-01), Research Foundation for the Electrotechnology of Chubu, Iketani Science and Technology Foundation, Collaborative Research Center on Energy Materials, Institute for Materials Research (IMR), Tohoku University, and the Cooperative Research Project of the Research Institute of Electric Communication, Tohoku University. The device fabrication, the film deposition by ion beam sputtering, and the XRD measurements were carried out at the Cooperative Research and Development Center for Advanced Materials, IMR, Tohoku University (Proposal Nos. 20G0415 and 202011-CRKEQ-0403).

AUTHOR DECLARATIONS

Conflict of Interest

The authors have no conflicts to disclose.

Author Contributions

Keita Ito: Conceptualization (lead); Data curation (lead); Formal analysis (lead); Funding acquisition (equal); Investigation (lead); Writing – original draft (lead); Writing – review & editing (equal). **Jian Wang:** Investigation (supporting); Writing – review & editing (equal). **Yusuke Shimada:** Investigation (supporting); Writing – review & editing (equal). **Himanshu Sharma:** Investigation (supporting); Writing – review & editing (equal). **Masaki Mizuguchi:** Funding acquisition (equal); Writing – review & editing (equal). **Koki Takanashi:** Funding acquisition (equal); Writing – review & editing (equal).

DATA AVAILABILITY

The data that support the findings of this study are available from the corresponding author upon reasonable request.

REFERENCES

[1]W. Nernst, "Ueber die electromotorischen Kräfte, welche durch den Magnetismus in von einem Wärmestrome durchflossenen Metallplatten geweckt warden," Ann. Phys. **267**, 760 (1887).

[2]Y. Sakuraba, K. Hasegawa, M. Mizuguchi, T. Kubota, S. Mizukami, T. Miyazaki, and K. Takanashi, "Anomalous Nernst effect in $L1_0$-FePt/MnGa thermopiles for New thermoelectric applications," Appl. Phys. Express **6**, 033003 (2013).

[3]Y. Sakuraba, "Potential of thermoelectric power generation using anomalous Nernst effect in magnetic materials," Scr. Mater. **111**, 29 (2016).

[4]M. Mizuguchi and S. Nakatsuji, "Energy-harvesting materials based on the anomalous Nernst effect," Sci. Technol. Adv. Mater. **20**, 262 (2019).

[5]K. Uchida, W. Zhou, and Y. Sakuraba, "Transverse thermoelectric generation using magnetic materials," Appl. Phys. Lett. **118**, 140504 (2021).

[6]R. Franz and G. Wiedemann, "Ueber die Wärme-Leitungsfähigkeit der Metalle," Ann. Phys. **165**, 497 (1853).

[7]W.-L. Lee, S. Watauchi, V. L. Miller, R. J. Cava, and N. P. Ong, "Anomalous Hall heat current and Nernst effect in the $CuCr_2Se_{4-x}Br_x$ ferromagnet," Phys. Rev. Lett. **93**, 226601 (2004).

[8]Y. Pu, D. Chiba, F. Matsukura, H. Ohno, and J. Shi, "Mott relation for anomalous Hall and Nernst effects in $Ga_{1-x}Mn_xAs$ ferromagnetic semiconductors," Phys. Rev. Lett. **101**, 117208 (2008).

[9]A. Sakai, S. Minami, T. Koretsune, T. Chen, T. Higo, Y. Wang, T. Nomoto, M. Hirayama, S. Miwa, D. N. Hamane, F. Ishii, R. Arita, and S. Nakatsuji, "Iron-based binary ferromagnets for transverse thermoelectric conversion," Nature **581**, 53 (2020).

[10]S. Isogami, K. Takanashi, and M. Mizuguchi, "Dependence of anomalous Nernst effect on crystal orientation in highly ordered γ'-Fe_4N films with anti-perovskite structure," Appl. Phys. Express **10**, 073005 (2017).

[11]H. P. R. Frederikse, W. R. Thurber, and W. R. Hosler, "Electronic transport in strontium titanate," Phys. Rev. **134**, A442 (1964).

[12]K. Ito, G. Hyoung Lee, H. Akinaga, and T. Suemasu, "Molecular beam epitaxy of ferromagnetic γ'-Fe_4N thin films on $LaAlO_3$(100), $SrTiO_3$(100) and MgO(100) substrates," J. Cryst. Growth **322**, 63 (2011).

[13]K. Ito, S. Higashikozono, F. Takata, T. Gushi, K. Toko, and T. Suemasu, "Growth and magnetic properties of epitaxial Fe_4N films on insulators possessing lattice spacing close to Si(001) plane," J. Cryst. Growth **455**, 66 (2016).

[14]J. Wang, Y.-C. Lau, W. Zhou, T. Seki, Y. Sakuraba, T. Kubota, K. Ito, and K. Takanashi, "Strain-induced large anomalous Nernst effect in polycrystalline Co_2MnGa/AlN multilayers," Adv. Electron. Mater. **8**, 2101380 (2022).

[15]T. Yamazaki, T. Seki, R. Modak, K. Nakagawara, T. Hirai, K. Ito, K. Uchida, and K. Takanashi, "Thickness dependence of anomalous Hall and Nernst effects in Ni-Fe thin films," Phys. Rev. B **105**, 214416 (2022).

[16]H. Reichlova, R. Schlitz, S. Beckert, P. Swekis, A. Markou, Y. C. Chen, D. Kriegner, S. Fabretti, G. Hyeon Park, A. Niemann, S. Sudheendra, A. Thomas, K. Nielsch, C. Felser, and S. T. B. Goennenwein, "Large anomalous Nernst effect in thin films of the Weyl semimetal Co_2MnGa," Appl. Phys. Lett. **113**, 212405 (2018).

[17]G. H. Park, H. Reichlova, R. Schlitz, M. Lammel, A. Markou, P. Swekis, P. Ritzinger, D. Kriegner, J. Noky, J. Gayles, Y. Sun, C. Felser, K. Nielsch, S. T. B. Goennenwein, and A. Thomas, "Thickness dependence of the anomalous Nernst effect and the Mott relation of Weyl semimetal Co_2MnGa thin films," Phys. Rev. B **101**, 060406 (2020).

[18]C. Yu, M. L. Scullin, M. Huijben, R. Ramesh, and A. Majumdar, "The influence of oxygen deficiency on the thermoelectric properties of strontium titanates," Appl. Phys. Lett. **92**, 092118 (2008).

[19]Y. Zhang, W. B. Mi, X. C. Wang, and X. X. Zhang, "Scaling of anomalous Hall effects in facing-target reactively sputtered Fe_4N films," Phys. Chem. Chem. Phys. **17**, 15435 (2015).

[20]K. Kabara, M. Tsunoda, and S. Kokado, "Anomalous Hall effects in pseudo-single-crystal γ'-Fe_4N thin films," AIP Adv. **6**, 055801 (2016).

[21]T. Miyasato, N. Abe, T. Fujii, A. Asamitsu, S. Onoda, Y. Onose, N. Nagaosa, and Y. Tokura, "Crossover behavior of the anomalous Hall effect and anomalous Nernst effect in itinerant ferromagnets," Phys. Rev. Lett. **99**, 086602 (2007).

[22]D. Kan, T. Terashima, R. Kanda, A. Masuno, K. Tanaka, S. Chu, H. Kan, A. Ishizumi, Y. Kanemitsu, Y. Shimakawa, and M. Takano, "Blue-light emission at room temperature from Ar^+-irradiated $SrTiO_3$," Nat. Mater. **4**, 816 (2005).

[23]M. L. Scullin, J. Ravichandran, C. Yu, M. Huijben, J. Seidel, A. Majumdar, and R. Ramesh, "Pulsed laser deposition-induced reduction of $SrTiO_3$ crystals," Acta Mater. **58**, 457 (2010).

[24]F. V. E. Hensling, D. J. Keeble, J. Zhu, S. Brose, C. Xu, F. Gunkel, S. Danylyuk, S. S. Nonnenmann, W. Egger, and R. Dittmann, "UV radiation enhanced oxygen vacancy formation caused by the PLD plasma plume," Sci. Rep. **8**, 8846 (2018).

[25]A. Viernstein, M. Kubicek, M. Morgenbesser, T. M. Huber, M. Siebenhofer, and J. Fleig, "How UV light lowers the conductivity of $SrTiO_3$ by photochemical water splitting at elevated temperature," Mater. Adv. **3**, 2800 (2022).

[26]D. Kan and Y. Shimakawa, "Strain effect on thermoelectric properties of $SrRuO_3$ epitaxial thin films," Appl. Phys. Lett. **115**, 022403 (2019).

[27]T. Seki, R. Iguchi, K. Takanashi, and K. Uchida, "Relationship between anomalous Ettingshausen effect and anomalous Nernst effect in an FePt thin film," J. Phys. D: Appl. Phys. **51**, 254001 (2018).

[28]W. Zhou and Y. Sakuraba, "Heat flux sensing by anomalous Nernst effect in Fe-Al thin films on a flexible substrate," Appl. Phys. Express **13**, 043001 (2020).

[29]H. Nakayama, K. Masuda, J. Wang, A. Miura, K. Uchida, M. Murata, and Y. Sakuraba, "Mechanism of strong enhancement of anomalous Nernst effect in Fe by Ga substitution," Phys. Rev. Mater. **3**, 114412 (2019).

[30]Y. Sakuraba, K. Hyodo, A. Sakuma, and S. Mitani, "Giant anomalous Nernst effect in the $Co_2MnAl_{1-x}Si_x$ Heusler alloy induced by Fermi level tuning and atomic ordering," Phys. Rev. B **101**, 134407 (2020).

[31]K. Uchida, T. Kikkawa, T. Seki, T. Oyake, J. Shiomi, Z. Qiu, K. Takanashi, and E. Saitoh, "Enhancement of anomalous Nernst effects in metallic multilayers free from proximity-induced magnetism," Phys. Rev. B **92**, 094414 (2015).

[32]C. Fang, C. H. Wan, Z. H. Yuan, L. Huang, X. Zhang, H. Wu, Q. T. Zhang, and X. F. Han, "Scaling relation between anomalous Nernst and Hall effect in $[Pt/Co]_n$ multilayers," Phys. Rev. B **93**, 054420 (2016).

[33]T. Seki, Y. Sakuraba, K. Masuda, A. Miura, M. Tsujikawa, K. Uchida, T. Kubota, Y. Miura, M. Shirai, and K. Takanashi, "Enhancement of the anomalous Nernst effect in Ni/Pt superlattices," Phys. Rev. B **103**, L020402 (2021).

[34]R. Kitaura, T. Ishibe, H. Sharma, M. Mizuguchi, and Y. Nakamura, "Nanostructure design for high performance thermoelectric materials based on anomalous Nernst effect using metal/semiconductor multilayer," Appl. Phys. Express **14**, 075002 (2021).

[35]S. Isogami, K. Masuda, Y. Miura, N. Rajamanickam, and Y. Sakuraba, "Anomalous Hall and Nernst effects in ferrimagnetic Mn_4N films: Possible interpretations and prospects for enhancement," Appl. Phys. Lett. **118**, 092407 (2021).